

## The AROME-France Convective-Scale Operational Model

Y. SEITY, P. BROUSSEAU, S. MALARDEL, G. HELLO, P. BÉNARD, F. BOUTTIER,  
C. LAC, AND V. MASSON

*Météo-France CNRM-GAME, Toulouse, France*

(Manuscript received 19 March 2010, in final form 29 September 2010)

### ABSTRACT

After six years of scientific, technical developments and meteorological validation, the Application of Research to Operations at Mesoscale (AROME-France) convective-scale model became operational at Météo-France at the end of 2008. This paper presents the main characteristics of this new numerical weather prediction system: the nonhydrostatic dynamical model core, detailed moist physics, and the associated three-dimensional variational data assimilation (3D-Var) scheme. Dynamics options settings and variables are explained. The physical parameterizations are depicted as well as their mutual interactions. The scale-specific features of the 3D-Var scheme are shown. The performance of the forecast model is evaluated using objective scores and case studies that highlight its benefits and weaknesses.

### 1. Introduction

Since the beginning of numerical weather prediction (NWP) in the 1950s, the resolution of models in national weather services has followed the progress of supercomputer capacities. At the turn of the millennium, the horizontal resolution of most operational limited-area models (LAM) was of the order of 10 km. Since the 1990s, research-oriented models such as Méso-NH (Lafore et al. 1998), the Weather Research and Forecasting model (WRF; Janjic 2003; Skamarock and Klemp 2008), or the fifth-generation Pennsylvania State University–National Center for Atmospheric Research (PSU–NCAR) Mesoscale Model (MM5; Grell et al. 1993) for instance, have demonstrated the potential of kilometric resolutions to improve operational forecasts in specific weather situations, such as flash flood events (Anquetin et al. 2005; Roberts et al. 2009; Davolio et al. 2009; Kain et al. 2006), or regional field experiments such as the Mesoscale Alpine Program (Richard et al. 2007). Flash flood events named “cévenols” occur frequently in late summer and during autumn in the southeast of France. They elicit some of the most devastating events in France, so there was a clear need for a NWP system that could better predict these events. In the cévenols context, Ducrocq

et al. (2002) have shown that mesoscale analysis could be even more important than lateral boundary conditions for a successful forecast of heavy rain patterns. The recent developments in supercomputers and observing systems now make it feasible to implement, for operational use, results from the most recent research in mesoscale models physics, dynamics, and data assimilation. A resolution of 2.5 km has been chosen in order to bypass the so-called convective gray zone (i.e., resolutions between 3 and 6 km); because deep convection is partly resolved by the model, but still needs to be partly parameterized as a subgrid process. This led to the Application of Research to Operations at Mesoscale (AROME-France) concept in France; similar to other European projects such as the German version of Consortium for Small Scale Modelling (COSMO) at 2.8-km resolution (Seifert et al. 2008) and the U.K. Unified Model at 4-km resolution (Davies et al. 2005), both of which have been operational since 2007.

AROME-France was declared operational on 18 December 2008, as a complement to the preexisting weather forecasting systems at Météo-France: the global Action de Recherche Petite Echelle Grande Echelle (ARPEGE; Courtier et al. 1994) system [which features a four-dimensional variational data assimilation (4D-Var) scheme and a stretched grid with a 15-km horizontal resolution over France], and the limited-area model Aire Limitée Adaptation Dynamique Développement International (ALADIN-France; Aladin International Team 1997) that covers western Europe at a 9.5-km

---

Corresponding author address: Yann Seity, Météo-France CNRM/GMAP, 42 av. G. Coriolis, 31057 Toulouse CEDEX, France.  
E-mail: yann.seity@meteo.fr

resolution. ALADIN-France takes its lateral boundary conditions from ARPEGE and its initial state from a three-dimensional variational data assimilation (3D-Var) scheme (Fischer et al. 2005). AROME-France, driven by ALADIN-France, provides a higher grid resolution over a smaller domain, in order to enhance the regional prediction of mesoscale phenomena.

The AROME project started at Météo-France in 2002 after a 2-yr feasibility study that focused on the intercomparison of dynamical cores. The AROME system backbone was then designed from a selection of the best available components available at the time, considerations of computational efficiency, and under the corporate constraint that the system had to be built and validated within 6 yr. The physical parameterizations were thus extracted from the Méso-NH research model (Lafore et al. 1998) and after some testing ALADIN-NH (Bubnová et al. 1995) was selected to provide the dynamical core of AROME. For this, the ALADIN-NH dynamical core had successfully passed a large variety of idealized test cases (not shown), such as vertical plane 2D simulations of orographic flows, including trapped lee waves (Keller 1994); bubble convection cases at decametric scales (Robert 1993); and 3D flows with and without earth rotation, over idealized and real orography, at various scales. At that stage, the building of AROME consisted mainly of interfacing part of the Méso-NH physics within the ALADIN-NH code. The prototype version of AROME first ran on some one-dimensional validation cases. The first 3D AROME model simulation ran in 2004, followed by extensive daily runs and validations over small areas until 2007, at which point, increasing computing capacities made real-time forecasts over the full French target domain possible. In late 2007, a 3D-Var scheme was implemented and replaced the previous procedure when AROME was running from an interpolated ALADIN analysis. The resulting experimental system was further improved, after 1 yr of intense daily scrutiny by forecasters and scientists. The following sections explain the key points of this development and validation process that led to a sound operational system.

The paper is organized as follow. Section 2 presents the dynamical core of the model, section 3 is devoted to the physical package, section 4 describes the data assimilation process, section 5 depicts the features of the current operational configuration, and section 6 provides some evaluation of the performance of the model. Conclusions are presented in section 7.

## 2. Adiabatic part

The hydrostatic hypothesis, better suited to larger-scale models, is relaxed in AROME, which solves the

nonhydrostatic (NH) fully compressible Euler Equations system (Bubnová et al. 1995). Some of the characteristics of AROME are shared with ALADIN. A two time level, semi-implicit (SI), semi-Lagrangian (SL) discretization scheme on an A grid is used. AROME is a spectral model: most prognostic variables have a spectral representation based on a double Fourier decomposition (assuming an extension zone for biperiodization of fields; Haugen and Machenhauer 1993; Radnóti 1995). Like ALADIN, AROME uses a mass-based hybrid pressure terrain-following coordinate  $\eta$  (Simmons and Burridge 1981; Laprise 1992). The vertical discretization is based on finite differences (Simmons and Burridge 1981). Note that there is no vertical staggering for any of the prognostic variables. This results in a single set of SL trajectories for all variables. The corresponding set of equations will not be described in this paper. The reader is referred to Bénard et al. (2010) for more details regarding the dynamical computations. AROME uses twelve 3D prognostic variables: 2 components of the horizontal wind ( $U$  and  $V$ ), temperature  $T$ , specific content of water vapor  $q_w$ , rain  $q_r$ , snow  $q_s$ , graupel  $q_g$ , cloud droplets  $q_c$ , ice crystals  $q_i$ , turbulent kinetic energy TKE, and two NH variables,  $\hat{q}$  and  $d$  that are related to pressure and vertical momentum (Bénard et al. 2010):

$$\hat{q} = \ln(p/\pi), \quad (1)$$

$$d = -g \frac{p}{(\partial\pi/\partial\eta)R_a T} \frac{\partial w}{\partial\eta} + \frac{p}{(\partial\pi/\partial\eta)RT} \nabla\phi \cdot \left( \frac{\partial\mathbf{V}}{\partial\eta} \right), \quad (2)$$

where  $p$  is the true pressure,  $\pi$  is the hydrostatic pressure,  $w$  is the vertical velocity, and  $R_a$  and  $R$  are the perfect gas constants of dry air and of the air–water vapor mixture, respectively. In addition, hydrostatic surface pressure is represented by a 2D prognostic variable  $\Pi_s$ . With this formulation, the equation system is consistently closed and the model is free of over specification for the evolution of the discrete state vector.

The temporal loop of the model is organized as follows: starting from the state vector in spectral space, an inverse bi-Fourier spectral transform is performed to go into grid point space. Then, the physical parameterization tendencies are computed and the SL transport scheme is applied, followed by dynamics computations needed as input to the SI step. The resulting grid point quantities are next converted into spectral space using direct bi-Fourier transforms. Afterward, the spectral part of numerical diffusion, the SI solver, and spatial derivatives are computed in spectral space in order to complete the time stepping.

In the SL advection, the use of quasi-monotonic operators averts the appearance of negative values for water condensate or TKE fields.

The spectral part of the diffusion is a fourth-order linear one, with the same strength for each spectral prognostic variable (e.g.,  $T$ , horizontal wind, vorticity, divergence,  $\hat{q}$ , and  $d$ ). The tuning of the numerical diffusion has been chosen to be as close as possible to the Méso-NH one so as to ensure as low as possible diffusion. The characteristic damping time for  $4\delta x$  waves is 2 h at the lowest level of the model; then the strength increases with height proportionally to the inverse of the pressure. As some prognostic variables (e.g., water condensates) are never converted into spectral space during the model integration, they cannot be diffused in the same way as the other prognostic variables. For water condensates, a so-called semi-Lagrangian horizontal diffusion (SLHD) nonlinear scheme (Vána et al. 2008) is applied. This scheme is implemented inside the SL scheme and uses information from the dynamical deformation field in order to diffuse the variables appropriately. The  $q_v$  and TKE variables are not diffused at all.

The lateral boundary coupling of AROME is performed using the Davies method (Radnóti 1995) on a relaxation zone with an eight-point width along the physical domain border. This very widespread coupling scheme is known to introduce some over specification, but the practical consequences are found to be acceptable provided the resolution gap between the host and guest models remains limited.

### 3. Physics

In this section we shall describe the physical parameterizations used in AROME and their interactions.

#### a. Microphysics

At 2.5-km horizontal resolution, a correct modeling of thunderstorms requires a mixed-phase microphysics scheme with riming processes and graupel. AROME uses a three-class ice parameterization (ICE3; Pinty and Jabouille 1998) Méso-NH microphysical scheme. ICE3 is coupled to a Kessler scheme for warm processes. It manages five prognostic variables of water condensates. In addition to water vapor specific content  $q_v$  it handles the prognostic specific contents of three precipitating species (rain  $q_r$ , snow  $q_s$  and graupel  $q_g$ ) and two non-precipitating species (ice crystals  $q_i$  and cloud droplets  $q_c$ ). In ICE3, hail is assumed to behave as large graupel particles. The diameter spectrum of each water species is assumed to follow a generalized Gamma distribution [simplified in a more classical exponential (or Marshall–Palmer) distribution for precipitating species]. Power-law

relationships are used to link the mass and the terminal speed velocity to the particle diameters. Microphysics prognostic variables are advected by the SL scheme. They act on inertia and gravity terms in the momentum equation and with their thermal inertia in the thermodynamical computations.

A more detailed documentation of the ICE3 microphysics scheme can be found in Lascaux et al. (2006). More than 25 processes are parameterized inside this scheme. They are treated explicitly, in a sequential way. The availability of each species is given by the sequence of the processes: the occurrence of a process is limited by the current state of the guess of the depleted prognostic variable before integration. The choice of the order of the processes, therefore, has a direct influence on the results.

The ICE3 scheme has been upgraded by two recent features: a subgrid condensation scheme, and a probability density function (PDF) based sedimentation scheme. The statistical subgrid condensation scheme (Bougeault 1982; Bechtold et al. 1995) is based on the computation of the variance of the departure from saturation inside the grid box diagnosed by the turbulence scheme. For instance, if the mean  $q_v$  does not reach saturation, whereas the variance is relatively high, then the diagnosed cloud fraction (which is not a prognostic variable of the model) and  $q_c$  could be different from zero.

The PDF-based sedimentation scheme has been developed in order to improve the numerical efficiency of the microphysics computation with relatively long time steps, as described in Bouteloup et al. (2011). The basic idea of the scheme is that for each falling hydrometeor, starting from the top layer of the model (where the incoming precipitating flux is 0.0), a budget is performed on each model layer, to compute the outgoing flux knowing the incoming flux and the hydrometeor content in the considered layer. The outgoing flux is the sum of a fraction ( $P_1$ ) of the incoming flux (corresponding to the fraction of incoming hydrometeor crossing the model layer in one time step), plus a fraction ( $P_2$ ) of the hydrometeor contained in the layer. Both  $P_1$  and  $P_2$  are computed by comparing the hydrometeors fall speed multiplied by the model time step (which corresponds to the traveled vertical distance) to the thickness of the layer. This last process of the microphysics is applied after the modification of species contents by other ICE3 processes.

#### b. Turbulence

The representation of the turbulence in the planetary boundary layer is based on a prognostic TKE equation combined with a diagnostic mixing length. The parameterization will enable computing the exchange coefficients

for momentum, potential temperature, and humidity, which in turn are used to compute the turbulent fluxes implicitly in time, through a tridiagonal matrix. The TKE scheme used in AROME was developed for Méso-NH by Cuxart et al. (2000), and uses the Bougeault and Lacarrere (1989) mixing length  $L$ . The  $L$  is computed from the distance traveled by an upward and downward adiabatic parcel before it is stopped at a level where it has lost all its TKE by buoyancy effects. It works with the following conservative variables: liquid potential temperature  $\theta_l$  and total specific content  $q_t$  (equal to  $q_v + q_c + q_i$ ). TKE is transported by the SL scheme.

### c. Surface

An externalized version of the Méso-NH surface scheme, called Externalized Surface (SURFEX), has been implemented in AROME. Each AROME grid box is split into four tiles: land, towns, sea, and inland waters (lakes and rivers). The Interactions between Soil, Biosphere, and Atmosphere (ISBA) parameterization (Noilhan and Planton 1989) with two vertical layers inside the ground is activated over land tile. The Town Energy Budget (TEB) scheme used for urban tiles (Masson 2000) simulates urban microclimate features, such as urban heat islands. Sea tiles use the Exchange Coefficients from Unified Multicampaigns Estimates (ECUME) parameterization (Belamari and Pirani 2007). It is a bulk iterative parameterization developed in order to obtain an optimized parameterization covering a wide range of atmospheric and oceanic conditions. Based on the Liu–Katsaros–Businger algorithm (Liu et al. 1979), ECUME includes an estimation of neutral transfer coefficients at 10 m from a multicampaign calibration derived from 5 flux measurement campaigns. Concerning inland waters, the classic Charnock's (Charnock 1955) formulation is used. Output fluxes are weight averaged inside each grid box according to the fraction occupied by each respective tile, before being provided to the atmospheric model. Physiographic data are initialized due to the ECOCLIMAP database (Masson et al. 2003) at 1-km resolution. The orographic setup is explained below.

The SURFEX scheme diagnoses the 2-m temperature, 2-m humidity, and 10-m wind at every time step due to a specific algorithm called Surface Boundary Layer (SBL) (Masson and Seity 2009). SBL implements a 1D prognostic-turbulence scheme on 6 vertical levels (0.5, 2, 4, 6.5, 10, and 17 m) inserted between the surface and the lowest atmospheric model level (which is 17 m above ground in the 2009 AROME operational version). This turbulence scheme predicts the evolution of TKE,  $U$ ,  $V$ ,  $q_v$ , and  $T$ , and provides screen level diagnostic values for these variables at a very fine vertical resolution. The same scheme as in atmospheric part is used (Cuxart

et al. 2000), but mixing and dissipative lengths are taken from Redelsberger et al. (2001; better adapted to surface boundary layer) instead of Bougeault and Lacarrere (1989). This approach implies that the atmospheric forcing to the surface is applied 0.5 m above ground, rather than at the lowest (17 m) 3D model level. As shown in Masson and Seity (2009), by using SBL, no decoupling occurs in stable conditions between the surface scheme and the atmospheric model, because of larger turbulent fluxes being simulated. Using SBL is a way to solve the problem of decoupling occurring in NWP models in stable conditions. With an additional cost of 3% of the total forecast, the SBL approach is numerically more costly than simpler diagnostic approaches, but remains cheaper than to apply this refined vertical resolution into the 3D atmospheric model (as vertical advection is neglected, there is no computational constraint near the bottom, arising from this refined resolution).

SURFEX is implemented as a model library that is formally free from the atmospheric model, and uses its own files for the initialization and the historic files production. The SURFEX orography could in principle be different from the one of the atmospheric model to which it is coupled. In AROME, the SURFEX orography is initialized with the one of the atmospheric model (in order to avoid issues with altitude inconsistencies). It is extracted from the Global 30 Arc-Second Elevation Data Set (GTOPO30) database (averaged at a  $0.0025^\circ$  resolution and from which  $2\text{-}\delta x$  waves are removed). Gibbs waves are filtered using Bouteloup (1995) algorithm.

### d. Radiation

AROME uses the European Centre for Medium-Range Weather Forecasts (ECMWF) radiation parameterizations. The shortwave radiation scheme (Fouquart and Bonnel 1980) uses six spectral bands. Cloud optical properties are derived from Morcrette and Fouquart (1986) for liquid clouds and Ebert and Curry (1992) for ice clouds. Cloud cover is computed in each column using the maximum cover value for sets of adjacent cloudy layers, and a random overlap assumption between cloudy layers separated by clear layers. The effective radius of liquid cloud particles is diagnosed from cloud liquid water using the Martin et al. (1994) formulation. Cloud nuclei concentrations are assumed to be constant, with one value over land and another over the ocean. The effective radius of ice clouds particles is diagnosed from temperature using a revision of the Ou and Liou (1995) formulation. Longwave radiation is computed by the Rapid Radiative Transfer Model (RRTM) code (Mlawer et al. 1997) using climatological distributions of ozone and aerosols. Ozone monthly profiles are given by analytical functions that have been fitted to the U.K. Universities

Global Atmospheric Modelling Programme (UGAMP) climatology (Li and Shine 1995) with three coefficients (Bouteloup and Toth 2003). The distributions of organic, sulfate, dust like and black carbon, plus uniformly distributed stratospheric background aerosols, are extracted from the Tegen climatology (Tegen et al. 1997). Because of computational constraints, only a part of the radiation parameterization, which is the shortwave flux dependency on the zenithal solar angle, is updated at every time step. Full radiation computations are performed once every 15 min.

#### e. Convection

At a 2.5-km resolution, the deep convection is assumed to be explicitly resolved by the model's dynamics. The shallow convection requires a parameterization of subgrid effect for which the Pergaud et al. (2009, hereafter PMMC09) scheme is used. It is a mass flux scheme based on the eddy diffusivity mass flux (EDMF) scheme (Soares et al. 2004) that parameterizes dry thermals and shallow cumuli. It uses the same conservative variables as the turbulence scheme ( $\theta_i$  and  $q_i$ ). The core of PMMC09 is the calculation of an updraft that represents the effect of the small updrafts within the model column, based on entrainment  $E$ –detrainment  $D$  formulations. In the boundary layer,  $E$  and  $D$  depend on the buoyancy and on the vertical speed of the updraft, whereas in clouds, they are computed using a Kain–Fritsch buoyancy sorting (Kain and Fritsch 1990). Compared to the original Kain–Fritsch scheme, this scheme improves the realism of PBL clouds and of winds in some situations. An example is shown in Fig. 1, with a modified version of AROME using the original Kain–Fritsch (Bechtold et al. 2001) shallow-convection scheme instead of PMMC09. This test simulation exhibits unrealistic low-level winds, linked to an organization of PBL eddies as “streets.” The current AROME model with PMMC09 avoids this problem because of a better representation of the counter-gradient zone in the upper boundary layer (and, to a lesser extent, better wind mixing by the mass flux). This leads to a smoother wind field, which is more realistic (it has been checked to be more consistent with observations).

#### f. Organization of physics computations

The AROME physics organization is shown in Fig. 2. Microphysics is divided into two parts. Within a model time step, physics computations start with a small part of the microphysics: a microphysics adjustment step. It diagnoses cloud fraction (which will be used by the radiation scheme) using information from a subgrid condensation scheme, and it enforces thermodynamic equilibrium between microphysical species concentration and the temperature field. Subsequent physics computations use

these so-called adjusted fields as input. Then, the radiation scheme is called. It provides input fluxes to the surface scheme. The surface scheme computes surface fluxes of potential temperature and water vapor (input to shallow convection and turbulence schemes) and surface fluxes of horizontal momentum (input to turbulence scheme). Surface radiative temperature, albedo, and emissivity, which will be used by radiative computations at the next time step are also computed by the surface scheme. Then, shallow convection computes two specific 3D output variables: a subgrid cloud droplets mixing ratio  $r_{c,\text{sub}}$ , and a subgrid cloud fraction  $cf_{\text{sub}}$ . They will be used at the following time-step adjustment call in which they will be added at the very end of the adjustment process to  $r_c$  and cloud fraction (indeed, if added before the adjustment, they would be re-evaporated during the adjustment process and the work of shallow convection scheme would be partly lost). The  $r_c$  is taken from the  $r_v$  reservoir and temperature is then modified according to  $r_v$  condensation. Then, the turbulence scheme is called, using as input the surface fluxes of wind stress, potential temperature  $\theta$ , and humidity. A 3D parameter used by the subgrid condensation scheme (see microphysics section), named *sigs* in Fig. 2, is stored. It corresponds to the variance of the departure from saturation, estimated by the turbulence scheme. It will be used by the microphysical adjustment at the next time step. Finally, the main part of the microphysics scheme is computed. The surface precipitations computed by the sedimentation algorithm are stored for use by the surface scheme at the following time step.

Radiation, turbulence, shallow convection, and microphysics parameterizations produce tendencies for the prognostic variables (e.g.,  $T$ , moist variables specific contents, wind, and TKE). The surface scheme only contributes to prognostic variables tendencies thanks to surface fluxes (of heat, momentum, and moisture) that are input to shallow convection and turbulence schemes. The influence of each physical parameterization on the model prognostic variables is displayed in the right-hand side of Fig. 2. Radiation, turbulence, shallow convection, and microphysics contributes to the tendency of  $T$ . Regarding hydrometeors, microphysics produces tendencies of  $q_x$  (with  $x = v, c, r, i, s, g$ ), turbulence acts on  $q_v, q_i$ , and  $q_c$ , and shallow convection acts on  $q_v$ . Shallow convection and turbulence contribute to wind tendencies, and turbulence contributes to TKE tendency.

#### 4. Initialization with mesoscale data assimilation

The AROME data assimilation system (Brousseau et al. 2008) is derived from the regional ALADIN-France 3D-Var scheme, which runs operationally at Météo-France

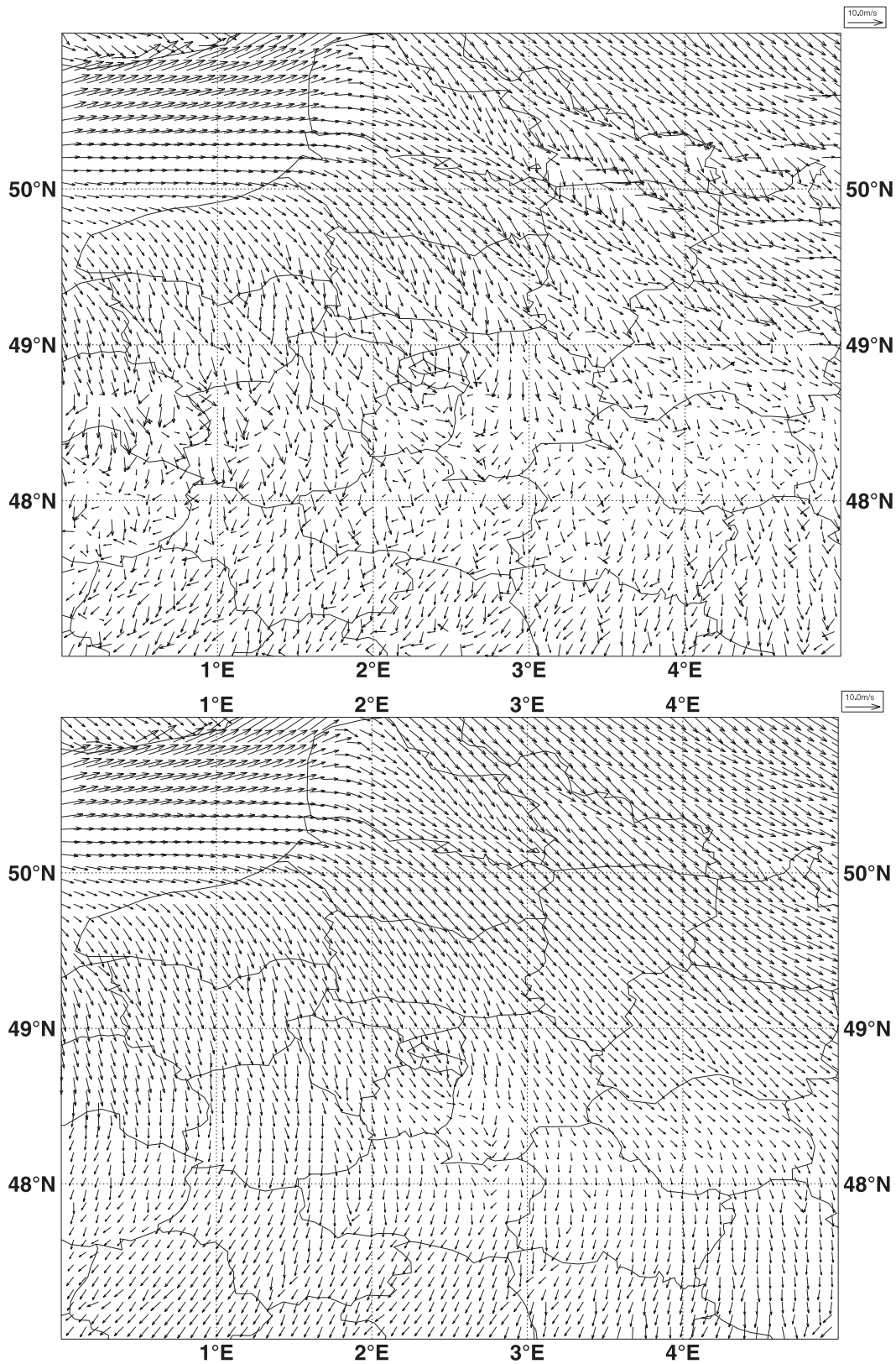


FIG. 1. The 30 Jul 2007 +15-h forecasts (starting at 0000 UTC) of lowest model level wind ( $m s^{-1}$ ) fields. With (top) Kain-Fritsch and (bottom) PMMC09 shallow convection schemes. Reference wind vector is plotted on the top right of (top) and (bottom).

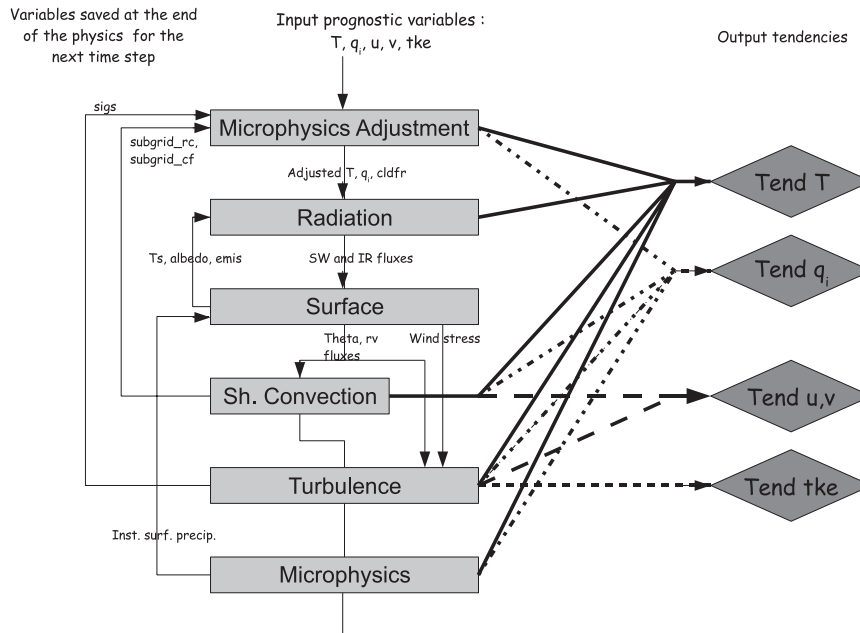


FIG. 2. AROME physics schematic.

since the end of 2005 (Fischer et al. 2005). This system inherits most of its characteristics of the ARPEGE-IFS software (Courtier et al. 1994; from which it has been developed). In particular, the incremental formulation, observations operators, minimization technique and data flow are nearly identical to the IFS-ARPEGE 3D-Var-4D-Var; although the latter was originally designed for large-scale analysis, it is well suited for mesoscale analysis, provided some adaptations are implemented. It is configured as a sequential 3D variational assimilation with 3-h cycles. Each 3D-Var analyzes the two components of the horizontal wind, the temperature, the specific humidity, and the surface pressure fields at the full 2.5-km model resolution. The other prognostic model fields (e.g., TKE, pressure departure, vertical divergence, and the five microphysical species) are not updated by the analyses. In other words, they are left to adjust themselves to the updated model fields during the forecast steps of the assimilation cycle.

#### a. Observations

Most observations used in the AROME data assimilation are shared with the ALADIN-France operational suite. The observations used are radiosondes, wind profilers, aircraft reports, ship and buoy reports, automated land surface stations (observations of pressure, 2-m temperature and humidity, 10-m wind), infrared radiances from Advanced Tiros Operational Vertical Sounder (ATOVS) and Spinning Enhanced Visible and Infrared Imager

(SEVIRI) satellite instruments, winds from atmospheric motion vectors (AMVs) and scatterometers, and GPS Zenith Tropospheric Delay (GPS-ZTD) observations from the European operational GPS network. For the time being, observations are used at the same spatial resolution as in ALADIN-France, except GPS-ZTD, which benefits from a specific station selection appropriate to the AROME resolution. Assimilating GPS-ZTD yields clear improvements in terms of quantitative precipitation forecasts (Yan et al. 2009; Boniface et al. 2009). In addition, AROME assimilates radial velocities from Doppler radars of the French network. Radar observations improve the spatial structure and the quantitative performance of precipitation forecasts because of better analyses of low-level convergence associated with convective systems (Montmerle and Faccani 2009). The assimilation of radar reflectivities is under development using a promising 1D+3DVar method (Caumont et al. 2010; Wattrelot et al. 2008). The number of observations used in each analysis is quite irregular during the day because, for example, radio soundings are performed only at 0000 and 1200 UTC in the AROME domain, and polar satellite orbits (ATOVS and scatterometers measurements) intersect the relatively small model domain only a few times a day. On the other hand, many important observing systems are abundant throughout the day at a high frequency, such as SYNOPs, aircraft, radar winds, and SEVIRI radiances. Montmerle et al. (2007) have, for instance, shown the usefulness of SEVIRI water vapor channel observations when there is a lack of

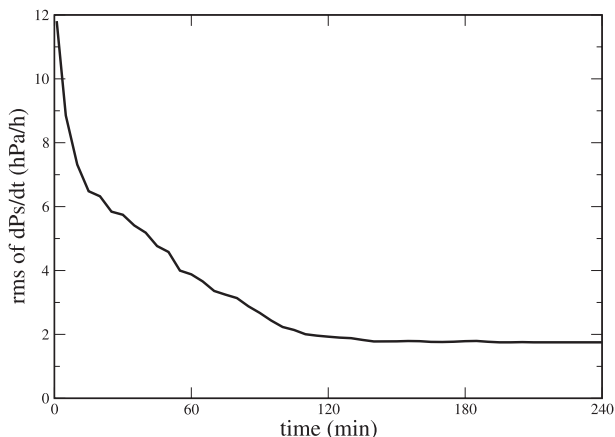


FIG. 3. Temporal evolution of the surface pressure tendency rms over a single time step (60 s) averaged over the model domain. Data points are taken every 5 min of integration.

High Resolution Infrared Radiation Sounder (HIRS) or Advanced Microwave Sounding Unit-B (AMSU-B) channels with comparable spectral responses. As previously demonstrated in the ALADIN-France assimilation, in the AROME 3DVar analysis step, the cost function gradient norm is reduced by a factor of 1000 in about 40 iterations of the minimization with a quasi-Newton algorithm M1QN3 (Gilbert and Lemaréchal 1989).

*b. Rapid Update Cycle*

The cycling strategy of the assimilation is designed to take full advantage of the high-density and high-frequency observations systems such as surface, GPS, and radar measurements. A way to alleviate the lack of a temporal dimension in the 3D-Var scheme is to use a rapid forward intermittent assimilation cycle such as the Rapid Update Cycle (RUC) that runs operationally at the National Centers for Environmental Prediction (NCEP) as described by Benjamin et al. (2004). These authors point out that a short assimilation cycle can

accumulate noise and imbalance in the analyses, which can degrade the forecast performance compared to a longer cycle. Figure 3 shows the temporal evolution of the root-mean-square of surface pressure tendency over the model domain, at each time step of an AROME forecast. The non meteorological values of this parameter in the first 2-h forecast range indicates that spurious tendencies are present in the model solution but are substantially reduced at the 3-h output time. Because initialization procedures like digital filter initialization (DFI; Lynch et al. 1997) to filter this model noise are not yet implemented in the AROME framework, the choice of a 3-h frequency assimilation cycle is made.

*c. Background error statistics*

The background error covariance model is an important scale-dependent aspect of the data assimilation system, because it determines how observations modify the background fields to produce the analysis. These covariances are estimated through the same multivariate formulation as ALADIN-France (Berre 2000) using forecast error statistics of vorticity, divergence, temperature, surface pressure, and specific humidity. Cross covariances are estimated using scale-dependent statistical regressions. An offline (i.e., non-real time) execution of a six-member AROME-France ensemble is used to compute climatological background error statistics over long periods (Berre et al. 2006). The AROME ensemble is perturbed through the use of initial and lateral conditions from an ARPEGE-ALADIN-France assimilation ensemble (Desroziers et al. 2008). Figure 4 shows a vertical cross section of temperature increments in single-observation experiments that use the same background fields, the same radiosonde temperature observation at level 850 hPa, and two different grid resolutions and background error statistics. The increment provided by AROME statistics (bottom panel) is more intense and more localized than the ALADIN-France increment (top

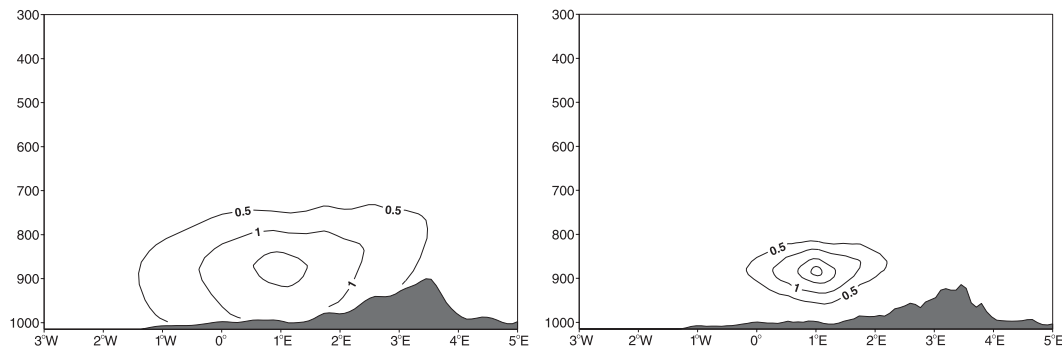


FIG. 4. Vertical cross section of temperature increments (contours every 0.5 K) due to a single radiosonde temperature observation at 875 hPa using (left) ALADIN-France and (right) AROME background error statistics. x axis: longitude (°). y axis: pressure (hPa).

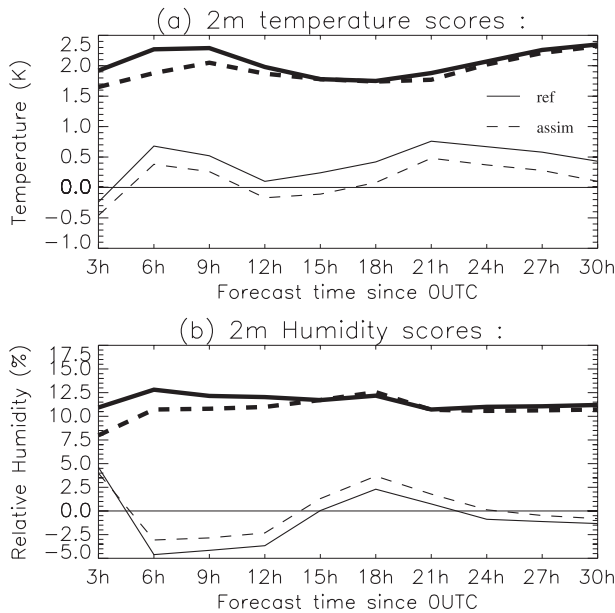


FIG. 5. Statistical scores vs observations (bias: thin lines; rmse: thick lines) of AROME forecasts initialized with ALADIN analyses (solid lines) and AROME analysis (dashed lines).

panel). The main reason for the incremental difference is the generally bigger background error variance in the AROME statistics, particularly in low atmospheric layers and at the smaller scales of divergence and vorticity. It appears to be consistent with the explicit representation of smaller-scale structures in AROME, such as deep convective towers, which are either absent or under-represented in ALADIN [see also Stăfănescu et al. (2006) for a similar comparison between ALADIN and ARPEGE background error statistics]. The existence of sharper correlations in AROME is also partly due to the smaller model domain. Sharp background error correlations imply that observing networks should have a good spatial coverage and geographical density in order to effectively control the behavior of the data assimilation system.

#### d. Impact of a mesoscale analysis

The usefulness of running a convective-scale data assimilation system is assessed by comparing the scores of forecasts that start either from AROME analyses, or from interpolated larger-scale ALADIN analyses. Both forecast sets use the same lateral boundary conditions. The scores are computed with respect to the low-level observations defined in section 6. All forecasts start at 0000 UTC. The scores plotted in Fig. 5 are a function of the forecast range. Using the AROME data assimilation provides a reduction of the forecast rmse, reaching 25% for the relative humidity and 15% for the temperature.

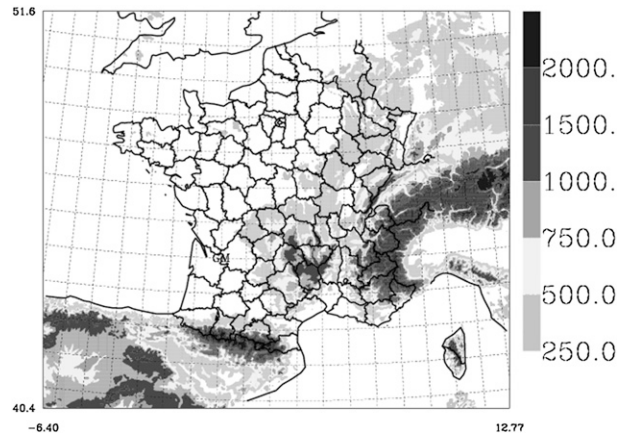


FIG. 6. Operational AROME-France domain.

Generally, the difference between the two sets of forecasts is significant during the first 12 h, then lateral boundary conditions largely take over the model solution and the two forecast sets become very close to each other in terms of scores. For the 0000 UTC analyses, this improvement mainly comes from the assimilation of nightly surface measurements by AROME, since ALADIN only assimilates them during daytime. A similar behavior is experienced with forecasts starting at 1200 UTC analyses (not shown), which demonstrates the benefit of assimilating small-scale features in AROME thanks to a high-resolution representation of orography, surface properties, and finescale background error correlation functions. Subjective evaluation by experienced forecasters confirms that analyses and short-range forecasts are improved, especially during the first 12 h, mainly in terms of localization of rain and fog events. Some weather conditions allow this benefit to be retained into longer ranges (e.g., in anticyclonic situations with fog), or a marked diurnal evolution of convection.

## 5. French operational configuration

The AROME model has been set up for operational production over the domain presented in Fig. 6. It is a regular 2.5-km grid on a Lambert projection, with its center at (46.4°N, 2.2°E), with 588 and 500 physical grid points in the east–west and north–south directions, respectively. An extra area of 12 points in both directions is added for the biperiodization of spectral fields. The domain is vertically divided in 41 layers, separated by hybrid pressure terrain-following  $\eta$  levels (Simmons and Burridge 1981). The center of the uppermost layer is located at 1 hPa. The height of the lowest layer center is about 17 m above the ground. Model fields are post-processed by interpolation of fields onto pressure or

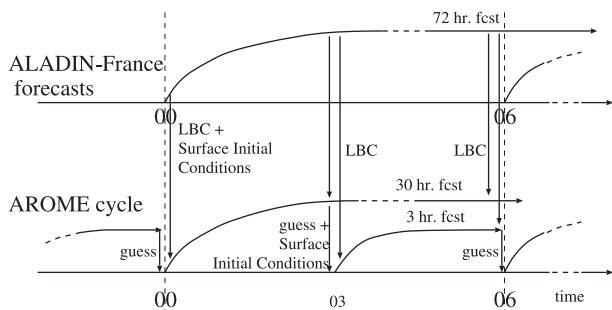


FIG. 7. Extract of the RUC scheme used in AROME.

altitude levels, and by computation of derived diagnostics such as simulated radar reflectivities and satellite images. In operation, this postprocessing is done on a regular latitude–longitude grid with a 0.025° resolution (about 2.5 km at 45°N). The model time step is 60 s. It has been checked that the model dynamics is stable and well behaved up to 90 s. A shorter time step is used to improve the precision of fast physical processes, particularly microphysics. Conversely, the full radiation scheme is only called every 15 min, which saves computing time without any noticeable penalty in accuracy.

The AROME operational suite uses a 3-hourly continuous assimilation cycle (Fig. 7). Each analysis is a 3D-Var with a 3-h assimilation window centered on the analysis time. Thirty-hour forecasts are issued from the 0000, 0600, 1200, and 1800 UTC nominal analysis times. The AROME model runs take hourly lateral boundary conditions from the latest available ALADIN-France forecasts. Surface fields conditions are updated at 0000, 0600, 1200, and 1800 UTC (only), using the ALADIN surface analysis (Giard and Bazile 2000). At other analysis times, the AROME background surface fields are used. For most of the analysis, the cutoff times (between the nominal analysis time and the start of the actual analysis computation) is 3.5 h. Because of operational constraints, it is shorter at 0000 UTC (1.2 h) and at 1200 UTC (2.3 h) than at other analysis times. Few observations are affected by this. Those that are affected are mostly observations near the end of the assimilation window, such as aircraft and polar-orbiting satellites measurements, for which the use of a short cutoff leads to a lack of observations of up to 40% compared to a longer one. Table 1 indicates the number of observations generally assimilated per analysis. On the Météo-France NEC-SX8R computer, the operational production uses 8 vector CPUs to compute each analysis step in 10 min, and 48 processors to issue forecasts at a rate of 24 h per 30 elapsed minutes. The profiling of forecast runs indicates that 40% of the elapsed time is spent in physics, 32% in interprocessor communications, and 16% in the semi-Lagrangian

TABLE 1. Mean number of observation assimilated in AROME-operational analysis.

Obs type	No. of assimilated obs
SYNOP + SHIP	1500
Radar	250–1000
Terrestrial GPS	170
Buoys	8
Radiosondes	20
Wind profilers	10
Aircrafts	15
Satellite-derived winds	15
HIRS	0–20
AMSU-A	0–20
AMSU-B	0–15
Diffusiometer winds	0–40
SEVIRI	150–300

advection of prognostic variables. The remainder is mostly spent in lateral boundary coupling, Fourier transforms, and semi-implicit dynamics calculations.

## 6. Evaluation of the model results

### a. Objective scores

An evaluation of the preoperational version of AROME was performed in 2008 as a comparison with the operational ALADIN-France forecasts. The truth is provided by an observing network made up of 18 radiosonde stations (available at 0000 and 1200 UTC over the AROME domain); 150 hourly ground-based observations of surface pressure; 1100 hourly ground based observations of 2-m temperature, 2-m humidity, and 10-m wind; and about 4000 observations of 24-h accumulated precipitations. In terms of radiosonde temperatures (Fig. 8), AROME improves the ALADIN forecasts with reduced biases at pressure levels greater than 300 hPa, and reduced RMSE at pressure greater than 700 hPa, with the strongest impact at midnight at level 1000 hPa. ALADIN has better scores than AROME in the high troposphere and low stratosphere. This is partly because the ALADIN vertical resolution is better than in AROME at these levels. The number of ground-based observations is much more significant. Scores of forecasts issued from 0000 UTC analyses (Fig. 9) show a similar behavior between AROME and ALADIN for 2-m temperature. AROME has a stronger positive bias in 10-m wind strength during the afternoon. It is related to an overestimation over mountains (not shown here). AROME improves the ALADIN forecasts in terms of daytime relative humidity and surface pressure. Forecasts issued from the 1200 UTC analyses lead to similar conclusions. The evaluation of precipitation tries to distinguish convective (in the summer) from mostly frontal type precipitations (in the autumn). In

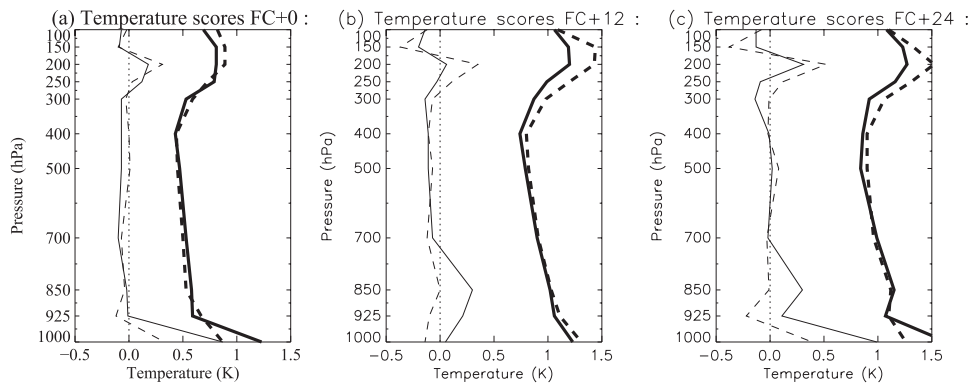


FIG. 8. Bias (thin lines) and rmse (thick lines) of AROME (dashed lines) and ALADIN (solid lines) temperature forecasted from 0000 UTC network, compared with radiosonde stations over AROME domain between 22 Sep and 7 Dec 2008: at (a) 0, (b) 12, and (c) 24 h.

order not to overly penalize the finer scale AROME forecasts because of slight delays in localization and/or timing with respect to observations (which will penalize twice the model in classic scores computations), specific scores adapted to mesoscale models are used (Amodei and Stein 2009). Brier skill score with a spatial tolerance of one verification grid point ( $0.2^\circ$ , about 30 km) is displayed in Fig. 10. AROME improvement is significant for light rains (below  $5 \text{ mm day}^{-1}$ ). It is stronger in summer period (in summer, the ALADIN deep-convection scheme had a tendency to trigger too often, leading to a positive bias in ALADIN light rains). For moderate and heavy rains, AROME and ALADIN behave similarly. A preoperational version of AROME has been evaluated and compared to other NWP mesoscale models during the Demonstration of Probabilistic Hydrological and Atmospheric Simulation of Flood Events in the Alpine region (D-PHASE; Rotach et al. 2009) and the Convective and Orographically induced Precipitation Study (COPS; Wulfmeyer et al. 2008) campaigns: the preoperational version of AROME had a strong positive bias in heavy rain distribution, which has been corrected in the operational version described in this paper.

#### b. Case study of a low clouds event: 26 February 2009

This situation is a typically stable case that occurs regularly in anticyclonic winter conditions. We compared AROME and ALADIN forecasts starting at 0600 UTC 25 February. After 27 h of forecast, Fig. 11 shows that AROME is able to capture low clouds areas over 1) Toulouse in the Garonne valley, 2) in the Ebro valley in Spain, and 3) around Montpellier, France. The white area in the center of Fig. 11 corresponds to snow cover over the Pyrénées. ALADIN only forecasts low clouds in the Ebro valley (not shown). The temporal evolution between 18 and 30 h of forecast time of 2-m temperature and humidity near Toulouse, France, is presented on

Fig. 12. In the observations, over Toulouse, low clouds appear at 0400 UTC and lift between 1000 and 1100 UTC. AROME with assimilation (ARO-oper) captures well the nocturnal cooling and the ensuing heating after sunrise. When low clouds are present, the relative humidity is slightly overestimated. AROME without data assimilation (ARO-dyn) does not perform as well as ARO-oper. For instance, temperature is underestimated by about  $1^\circ$  or  $2^\circ\text{C}$  after 0500 UTC. ALADIN (without low clouds over Toulouse) forecast cooler temperature during the night (clear sky leads to an overestimation of radiative cooling), and conversely too hot temperatures after sunrise due to solar heating. ALADIN 2-m relative humidity is stronger than the AROME one, but it is the reverse just above at model levels (not shown).

#### c. Case study of a convective event: 4 September 2008

Ahead of a trough located over the United Kingdom, a southwesterly flow blew over France, with moist and unstable air in the southeastern part of France. During the day, a secondary trough in the upper troposphere crossed the southern part of France, favoring the triggering of a strong convective event in this area. Hailstones of up to 3-cm diameter have been reported under the strongest cells having thunder causing damage over an area of  $50 \text{ km}^2$  near Montpellier, especially to many vineyards. Gusts stronger than  $100 \text{ km h}^{-1}$ , an F1 tornado associated with a supercell, strong electric activity with sometimes more than 200 lightning strikes per minute and exceptional rainfall rates (as much as  $101 \text{ mm}$  in 1 h) were observed. At 1900 UTC, observation from the Nîmes French radar (Fig. 13) showed a hook shape that was characteristic of a supercell and reflectivities higher than 60 dBZ (very probably associated with hail). This hook shape is observed between 1815 and 1915 UTC. A strong thunder-producing cell was also forecast by the 0000 UTC AROME run, even if delayed by 2 h (Fig. 14).

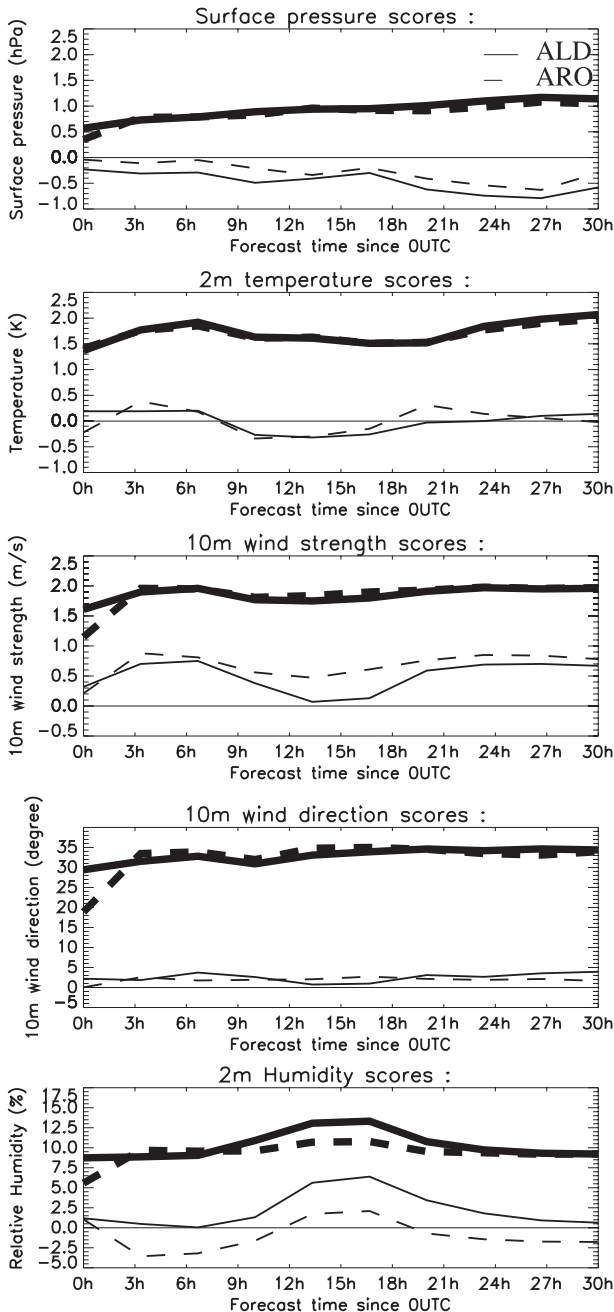


FIG. 9. Comparative scores of bias (thin lines) and rmse (thick lines) from AROME (dashed lines) and ALADIN (solid lines) 0000 UTC network forecasts between 22 Sep and 7 Dec 2008. The reference is the French surface observation network: (top to bottom) surface pressure, 2-m temperature, 10-m wind speed, 10-m wind direction, and 2-m relative humidity.

The 0000 UTC ALADIN run did not forecast any convection. The AROME time delay was reduced in the next AROME forecasts (starting at 0600 or 1200 UTC) whereas ALADIN was still not able to forecast any rain for the area. The typical size of the thunder-producing cell was

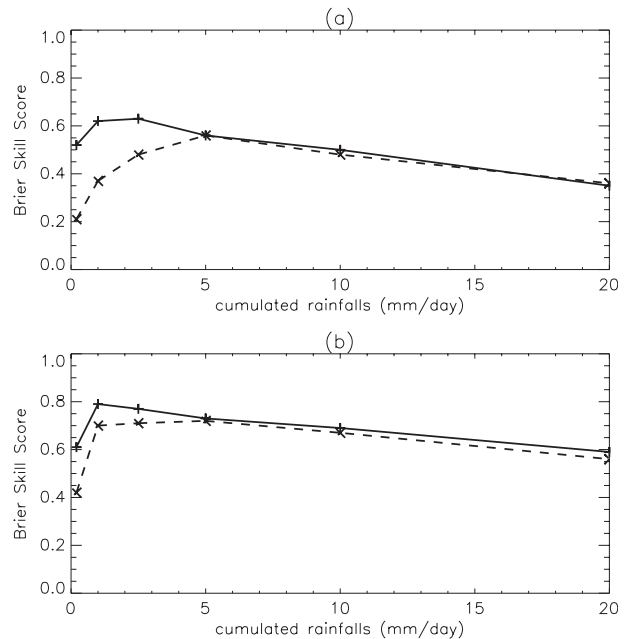


FIG. 10. Brier skill score relative to persistence, with a tolerance of 1 verification grid point, for different thresholds of 24-h cumulative rainfalls: ALADIN (dashed lines) and AROME (solid lines) for (a) 2 Jun–10 Sep 2008 and (b) 11 Sep–31 Oct 2008.

about 35 km in the observations and 50 km in AROME. Strong rain rates are diagnosed by AROME. In Fig. 14, wind field exhibits a strong convergence of southeasterly winds coming from the Mediterranean sea in front of the cell and northwesterly winds at the rear. A simulated vertical profile (Fig. 15) just in front of the cell showed the instability of the air, with a CAPE of  $2167 \text{ J kg}^{-1}$ . We can notice a strong vertical wind shear, from the east at the

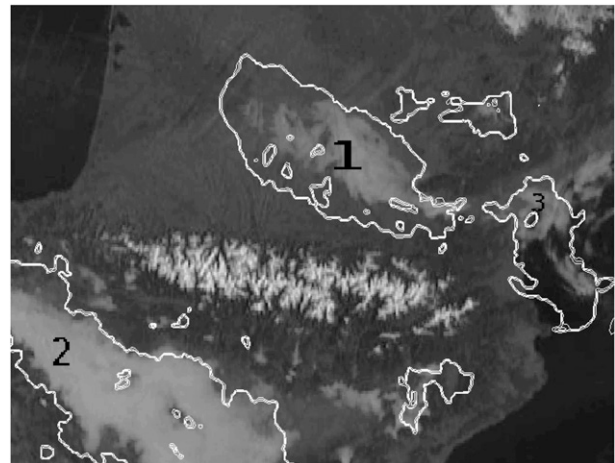


FIG. 11. Satellite observation of low clouds over the southwestern part of France at 0900 UTC 26 Feb 2009 that corresponds to the AROME + 27-h forecast (white contour).

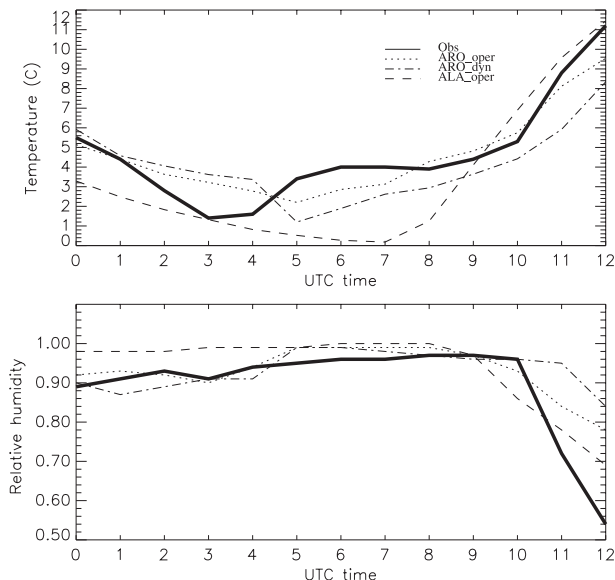


FIG. 12. Time evolution of 2-m (top) temperature and (bottom) relative humidity at Toulouse-Blagnac, France on 26 Feb 2009.

bottom to the west at the top of the cloud, and a strong strengthening of the wind with altitude. Model helicity calculations gave values of about  $300 \text{ m}^2 \text{ s}^{-2}$ , which are values reported for supercells. Dry air was present in the environment at low levels, favoring the evaporation of the rain (not shown). Thanks to a cross section through the most intense thunder-producing cell (Fig. 16), we could verify that the model reproduced the classic features of

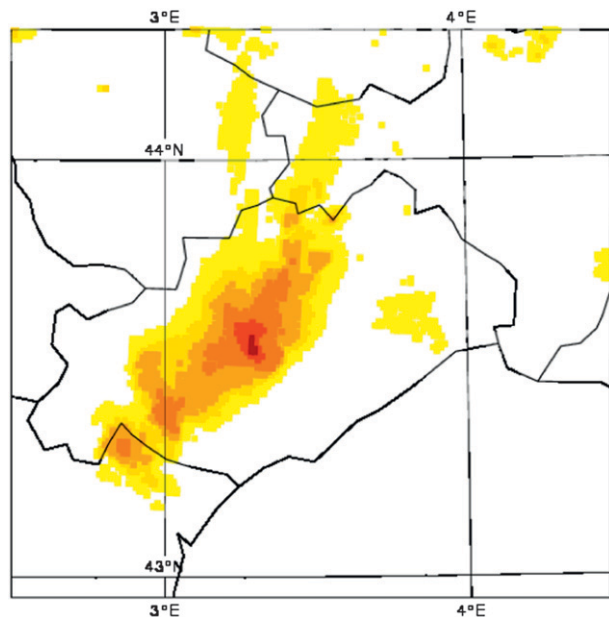


FIG. 13. The 1900 UTC Nimes radar observation ( $\text{mm h}^{-1}$ ) over the Herault, France, department (same color scale as in Fig. 14).

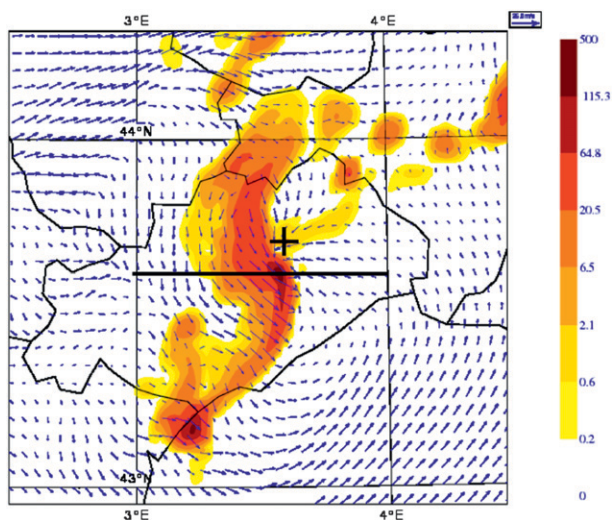


FIG. 14. The 2100 UTC AROME horizontal wind ( $\text{m s}^{-1}$ ) and simulated radar reflectivity ( $\text{mm h}^{-1}$ ) at 1000-m height in the area of Montpellier, France. The black cross indicates the location of the profile in Fig. 15, and the thick line denotes the vertical cross section in Fig. 16.

strong cells that have thunder: a strong ascent with a maximum value of about  $25 \text{ m s}^{-1}$ , the development of an anvil at the top of the cloud with an overshoot just on top of the convective ascent, and heavy rain with  $q_r$

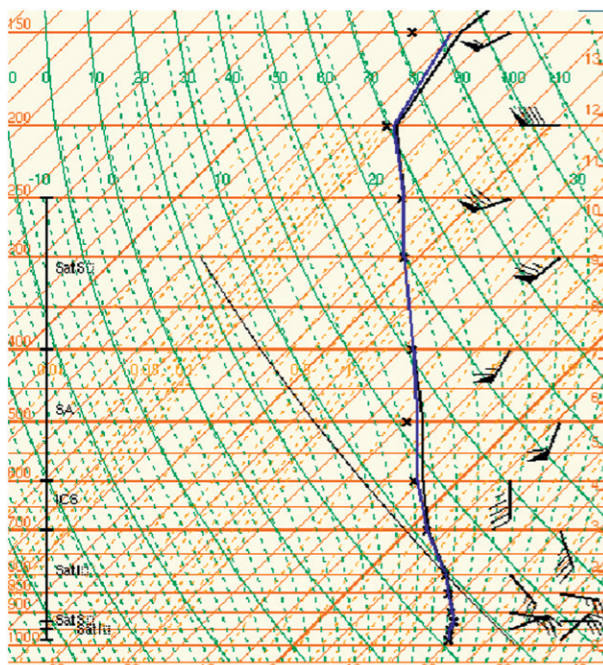


FIG. 15. The AROME vertical profile (temperature and wet bulb temperature) in the cloudy area just in front of the most intense thunder cell at 2100 UTC (see location in Fig. 14). Crosses indicate dewpoint temperature.

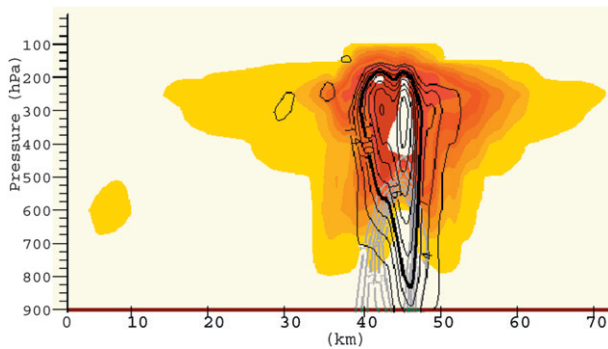


FIG. 16. Vertical crosssection through the most intense thunder cell at 2100 UTC (axis depicted in Fig. 14). Snow content is in shades ( $0.5 \text{ g kg}^{-1}$  steps starting at  $0.01 \text{ g kg}^{-1}$ ), vertical velocities are in black contours, and rain content is in gray contours.

up to  $9 \text{ g kg}^{-1}$ . AROME is not able to forecast hail directly (as it is not one of its prognostic variable), but a strong content of graupel ( $7.3 \text{ g kg}^{-1}$ ) was sustained by the strong vertical velocities (not shown). Nevertheless, they did not reach the ground as they melted below 800 hPa (temperature about  $10^\circ\text{C}$  at that level). With a 2-h delay and a slightly overestimated horizontal size and intensity, AROME was able to reproduce the main characteristics of this stormy day in the south of France.

## 7. Conclusions and outlook

The three main components of the AROME 2.5-km model are its nonhydrostatic dynamics inherited from ALADIN, its mesoscale physics mostly coming from Méso-NH, and its 3D-Var scheme with some mesoscale specific data such as Doppler radar winds. The way it is built, the AROME model has proved beneficial for forecasts over France by a day-to-day evaluation and automatic scores calculations. It was declared valid for operational use at Météo-France in December 2008. Indeed, in spite of marginal improvements in terms of scores compared to ALADIN forecasts, AROME forecasts often provide better physical realism, which can be attributed to its mesoscale physics-dynamics and data assimilation scheme. AROME seems to be more accurate than ALADIN in predicting the finescale structure of low-level moist processes (fog) and convective processes. Nevertheless, this first version can be improved. For example, we suspect that the model tends to overestimate the horizontal size of convective cells and we are trying to understand this behavior.

By the end of 2010, thanks to a new version of the supercomputer, and some research–development work, the following operational evolutions are planned: (i) the low-level vertical resolution of the model will be improved by using at least 60 vertical levels; the lowest one will be at

10 m and there will be 28 levels below 3000 m (instead of 16 in the 41 levels distribution; this change will improve the forecasts of low clouds and fog); (ii) the sedimentation of fog will be activated in order to improve the dissipation of very thin fogs especially over sea; (iii) radar reflectivities will be assimilated as it already exhibits promising results in research mode (Caumont et al. 2010; Wattrelot et al. 2008); and (iv) a flow dependency in background error statistics using information from an ARPEGE ensemble assimilation will be introduced.

In parallel, some options will be evaluated, among them: (i) the testing of some changes in the microphysical scheme (activation of hail as a new prognostic variable; Lascaux et al. 2006); (ii) a direct coupling with ARPEGE as its resolution will reach 10 km over France in 2010; and (iii) the addition of a surface analysis consistent with the SURFEX physics in the assimilation process.

In the long term, more advanced methods of coupling (Boyd 2005) and AROME behavior at 1-km or 500-m resolution are under investigation. A prototype version at 1-km resolution has been used and positively evaluated by forecasters during the ski world championship in Val d'Isère, France, in February 2009. The need for 3D physics (especially turbulence) at that resolution remains open. Evaluations of ensemble mesoscale forecasts with AROME are also planned. Concerning the data assimilation system, ways to increase the temporal resolution of assimilated observations will be investigated using higher frequency of the assimilation cycle and/or the 3D first guess at appropriate time (FGAT) scheme. Ensemble assimilation techniques will be used in order to specify flow-dependent and heterogeneous background error statistics. Moreover, as a research version of AROME, according to an online coupling, chemistry (Tulet et al. 2003), the Organic Inorganic Lognormal Aerosol Model (ORILAM) anthropogenic aerosols (Tulet et al. 2005), and desert dusts (Grini et al. 2006) modules of Méso-NH has been included and could be switched on for research purposes.

*Acknowledgments.* We wish to thank J.-A. Maziejewski for his help in revising the manuscript.

## REFERENCES

- Aladin International Team, 1997: The Aladin project mesoscale modelling seen as basic tool for weather forecasting and atmospheric research. *WMO Bull.*, **46**, 317–324.
- Amodei, M., and J. Stein, 2009: Deterministic and fuzzy verification methods for a hierarchy of numerical models. *Meteor. Appl.*, **16**, 191–203.
- Anquetin, S., and Coauthors, 2005: The 8 and 9 September 2002 flash flood event in France: A model intercomparison. *Nat. Hazards Earth Syst.*, **5**, 741–754.

- Bechtold, P., J. Cuijpers, P. Mascart, and P. Trouilhet, 1995: Modelling of trade-wind cumuli with a low-order turbulence model—toward a unified description of Cu and Sc clouds in meteorological models. *J. Atmos. Sci.*, **52**, 455–463.
- , E. Bazile, F. Guichard, P. Mascart, and E. Richard, 2001: A mass-flux convection scheme for regional and global models. *Quart. J. Roy. Meteor. Soc.*, **127**, 869–886.
- Belamari, S., and A. Pirani, 2007: Validation of the optimal heat and momentum fluxes using the ORCA2-LIM global ocean-ice model. Marine environment and security for the European area. Integrated Project (MERSEA IP), Deliverable D4.1.3, 88 pp.
- Bénard, P., J. Vivoda, J. Mašek, P. Smolíková, K. Yessad, C. Smith, R. Brožková, and J.-F. Geleyn, 2010: Dynamical kernel of the Aladin-NH spectral limited-area model: Revised formulation and sensitivity experiments. *Quart. J. Roy. Meteor. Soc.*, **136**, 155–169.
- Benjamin, S. G., and Coauthors, 2004: An hourly assimilation-forecast cycle: The RUC. *Mon. Wea. Rev.*, **132**, 495–518.
- Berre, L., 2000: Estimation of synoptic and mesoscale forecast error covariances in a limited-area model. *Mon. Wea. Rev.*, **128**, 644–667.
- , S. E. Ștefănescu, and M. B. Pereira, 2006: The representative of the analysis effect in three error simulation techniques. *Tellus*, **58A**, 196–209.
- Boniface, K., V. Ducrocq, G. Jaubert, X. Yan, P. Brousseau, F. Masson, J. Chéry, and E. Doerflinger, 2009: Impact of high-resolution data assimilation of GPS zenith delay assimilation on Mediterranean heavy rainfall forecasting. *Ann. Geophys.*, **27**, 2739–2753.
- Bougeault, P., 1982: Cloud-ensemble relations based on the gamma probability distribution for the higher-order models of the planetary boundary layer. *J. Atmos. Sci.*, **39**, 2691–2700.
- , and P. Lacarrere, 1989: Parameterization of orography-induced turbulence in a meso-beta-scale model. *Mon. Wea. Rev.*, **117**, 1870–1888.
- Bouteloup, Y., 1995: Improvement of the spectral representation of the earth topography with a variational method. *Mon. Wea. Rev.*, **123**, 1560–1573.
- , and H. Toth, 2003: Refinements in the parameterisation of radiative exchanges. *ALADIN Newsl.*, **23**, 178–183.
- , Y. Seity, and E. Bazile, 2011: Description of the PDF based sedimentation scheme used in operation in all Météo-France NWP models. *Tellus*, in press.
- Boyd, J. P., 2005: Limited-area Fourier spectral models and data analysis schemes: Windows, Fourier extension, Davies relaxation, and all that. *Mon. Wea. Rev.*, **133**, 2030–2042.
- Brousseau, P., and Coauthors, 2008: A prototype convective-scale data assimilation system for operation: The AROME-RUC. HIRLAM Tech. Rep. 68, 23–30.
- Bubnová, R., G. Hello, P. Bénard, and J.-F. Geleyn, 1995: Integration of the fully elastic equations cast in the hydrostatic pressure terrain-following in the framework of the ARPEGE/ALADIN NWP system. *Mon. Wea. Rev.*, **123**, 515–535.
- Caumont, O., V. Ducrocq, E. Wattrelot, G. Jaubert, and S. Pradier-Vabre, 2010: 1D+3DVar assimilation of radar reflectivity data: A proof of concept. *Tellus*, **62**, 173–187.
- Charnock, H., 1955: Wind stress over a water surface. *Quart. J. Roy. Meteor. Soc.*, **81**, 639–640.
- Courtier, P., J.-N. Thépaut, and A. Hollingsworth, 1994: A strategy for operational implementation of 4D-VAR using an incremental approach. *Quart. J. Roy. Meteor. Soc.*, **120**, 1367–1387.
- Cuxart, J., P. Bougeault, and J.-L. Redelsberger, 2000: A turbulence scheme allowing for mesoscale and large-eddy simulations. *Quart. J. Roy. Meteor. Soc.*, **126**, 1–30.
- Davies, T., M. J. P. Cullen, A. J. Malcolm, M. H. Mawson, A. Staniforth, A. A. White, and N. Wood, 2005: A new dynamical core for the Met Office's global and regional modelling of the atmosphere. *Quart. J. Roy. Meteor. Soc.*, **131**, 1759–1782.
- Davolio, S., D. Mastrangelo, M. M. Miglietta, O. Drofa, A. Buzzi, and P. Malguzzi, 2009: High resolution simulations of a flash flood near Venice. *Nat. Hazards Earth Syst.*, **9**, 1671–1678.
- Desroziers, G., L. Berre, O. Pannekoucke, S. Ștefănescu, P. Brousseau, L. Auger, B. Chapnik, and L. Raynaud, 2008: Flow-dependant error covariances from variational assimilation ensembles on global and regional domains. HIRLAM Tech. Rep. 68, 2–22.
- Ducrocq, V., D. Richard, J.-P. Lafore, and F. Orain, 2002: Storm-scale numerical rainfall prediction for five precipitating events over France: On the importance of initial humidity field. *Wea. Forecasting*, **17**, 1236–1256.
- Ebert, E., and J. A. Curry, 1992: A parameterization of ice cloud optical properties for climate models. *J. Geophys. Res.*, **97**, 3831–3835.
- Fischer, C., T. Montmerle, L. Berre, L. Auger, and S. E. Ștefănescu, 2005: An overview of the variational assimilation in the Aladin/France NWP system. *Quart. J. Roy. Meteor. Soc.*, **131**, 3477–3492.
- Fouquart, Y., and B. Bonnel, 1980: Computations of solar heating of the earth's atmosphere: A new parameterization. *Beitr. Phys. Atmos.*, **53**, 35–62.
- Giard, D., and E. Bazile, 2000: Implementation of a new assimilation scheme for soil and surface variables in a global NWP model. *Mon. Wea. Rev.*, **128**, 997–1015.
- Gilbert, J., and C. Lemaréchal, 1989: Some numerical experiments with variable storage quasi-Newton algorithms. *Math. Program.*, **B25**, 407–435.
- Grell, G., J. Dudhia, and D. Stauffer, 1993: A description of fifth-generation Penn State/NCAR mesoscale model (MM5). NCAR Tech. Note 398, 117 pp.
- Grimi, A., P. Tulet, and L. Gomes, 2006: Dusty weather forecasts using the MesoNH mesoscale atmospheric model. *J. Geophys. Res.*, **111**, D19205, doi:10.1029/2005JD007007.
- Haugen, J., and B. Machenhauer, 1993: A spectral limited-area model formulation with time-dependent boundary conditions applied to shallow-water equations. *Mon. Wea. Rev.*, **121**, 2618–2630.
- Janjic, Z. I., 2003: A nonhydrostatic model based on a new approach. *Meteor. Atmos. Phys.*, **82**, 271–285.
- Kain, J. S., and J. M. Fritsch, 1990: A one-dimensional entraining/detraining plume model and its application in convective parameterizations. *J. Atmos. Sci.*, **47**, 2784–2802.
- , S. J. Weiss, J. J. Levit, M. E. Baldwin, and D. R. Bright, 2006: Examination of convection-allowing configurations of the WRF model for the prediction of severe convective weather: The SPC/NSSL spring program 2004. *Wea. Forecasting*, **21**, 167–181.
- Keller, T. L., 1994: Implications of the hydrostatic assumption on atmospheric gravity waves. *J. Atmos. Sci.*, **51**, 1915–1929.
- Lafore, J.-P., and Coauthors, 1998: The Meso-NH atmospheric simulation system. Part I: Adiabatic formulation and control simulations. *Ann. Geophys.*, **16**, 90–109.
- Laprise, R., 1992: The Euler equations of motion with hydrostatic pressure as an independent variable. *Mon. Wea. Rev.*, **120**, 197–207.
- Lascaux, F., E. Richard, and J.-P. Pinty, 2006: Numerical simulations of three map IOPs and the associated microphysical processes. *Quart. J. Roy. Meteor. Soc.*, **132**, 1907–1926.

- Li, D., and K. P. Shine, 1995: A 4-dimensional ozone climatology for UGAMP models. UGAMP Internal Rep. 35.
- Liu, W. T., K. B. Katsaros, and A. Businger, 1979: Bulk parameterization of air–sea exchanges of heat and water vapor including the molecular constraints at the interface. *J. Atmos. Sci.*, **36**, 1722–1735.
- Lynch, P., D. Giard, and V. Ivanovici, 1997: Improving the efficiency of a digital filtering scheme for diabatic initialization. *Mon. Wea. Rev.*, **125**, 1976–1982.
- Martin, G. M., D. W. Johnson, and A. Spice, 1994: The measurement and parameterization of effective radius of droplets in warm stratocumulus. *J. Atmos. Sci.*, **51**, 1823–1842.
- Masson, V., 2000: A physically-based scheme for the urban energy budget in atmospheric models. *Bound.-Layer Meteor.*, **94**, 357–397.
- , and Y. Seity, 2009: Including atmospheric layers in vegetation and urban offline surface schemes. *J. Appl. Meteor. Climatol.*, **48**, 1377–1397.
- , J.-L. Champeaux, F. Chauvin, C. Meriguet, and R. Lacaze, 2003: A global database of land surface parameters at 1-km resolution in meteorological and climate models. *J. Climate*, **16**, 1261–1282.
- Mlawer, E. J., S. J. Taubman, P. Brown, M. J. Iacono, and S. A. Clough, 1997: Radiative transfer for inhomogeneous atmospheres: RRTM, a validated correlated-k model for the longwave. *J. Geophys. Res.*, **102**, 16 663–16 682.
- Montmerle, T., and C. Faccani, 2009: Mesoscale assimilation of radial velocities from Doppler radars in a preoperational framework. *Mon. Wea. Rev.*, **137**, 1939–1953.
- , F. Rabier, and C. Fischer, 2007: Relative impact of polar-orbiting and geostationary satellite radiances in the Aladin/France numerical weather prediction system. *Quart. J. Roy. Meteor. Soc.*, **133**, 655–671.
- Morcrette, J.-J., and Y. Fouquart, 1986: The overlapping of cloud layers in shortwave radiation parameterizations. *J. Atmos. Sci.*, **43**, 321–328.
- Noilhan, J., and S. Planton, 1989: simple parameterization of land surface processes for meteorological models. *Mon. Wea. Rev.*, **117**, 536–549.
- Ou, S. C., and K.-N. Liou, 1995: Ice microphysics and climatic temperature feedback. *Atmos. Res.*, **35**, 127–138.
- Pergaud, J., V. Masson, S. Malardel, and F. Couvreux, 2009: A parameterization of dry thermals and shallow cumuli for mesoscale numerical weather prediction. *Bound.-Layer Meteor.*, **132**, 83–106.
- Pinty, J.-P., and P. Jabouille, 1998: A mixed-phased cloud parameterization for use in a mesoscale non-hydrostatic model: Simulations of a squall line and of orographic precipitation. Preprints, *Conf. on Cloud Physics*, Everett, WA, Amer. Meteor. Soc., 217–220.
- Radnóti, G., 1995: Comments on “A spectral limited-area formulation with time-dependent boundary conditions for the shallow-water equations.” *Mon. Wea. Rev.*, **123**, 3122–3123.
- Redelsberger, J.-L., F. Mahe, and P. Carlotti, 2001: A simple and general subgrid model suitable both for surface layer and free-stream turbulence. *Bound.-Layer Meteor.*, **101**, 375–408.
- Richard, E., A. Buzzi, and G. Zängl, 2007: Quantitative precipitation forecasting in the Alps: The advances achieved by the Mesoscale Alpine Programme. *Quart. J. Roy. Meteor. Soc.*, **133**, 831–846.
- Robert, A., 1993: Bubble convection experiments with a semi-implicit formulation of the Euler equations. *J. Atmos. Sci.*, **50**, 1865–1873.
- Roberts, N. M., S. J. Cole, R. M. Forbes, R. J. Moore, and D. Boswell, 2009: Use of high-resolution NWP rainfall and river flow forecasts for advance warning of the Carlisle flood, northwest England. *Meteor. Appl.*, **16**, 23–34.
- Rotach, M. W., and Coauthors, 2009: MAP D-PHASE: Real-time demonstration of weather forecast quality in the Alpine region. *Bull. Amer. Meteor. Soc.*, **90**, 1321–1336.
- Seifert, A., M. Baldauf, K. Stephan, U. Blahak, and K. Beheng, 2008: The challenge of convective-scale quantitative precipitation forecasting. *15th Int. Conf. on Clouds and Precipitation*, Cancun, Mexico, Centro de Ciencias de la Atmósfera, Universidad Nacional Autónoma de México (CCA-UNAM).
- Simmons, A., and D. M. Burridge, 1981: An energy and angular-momentum conserving finite-difference scheme and hybrid vertical coordinates. *Mon. Wea. Rev.*, **109**, 758–766.
- Skamarock, W. C., and J. B. Klemp, 2008: A time-split nonhydrostatic atmospheric model for weather research and forecasting applications. *J. Comput. Phys.*, **227**, 3465–3485.
- Soares, P. M. M., P. M. A. Miranda, A. P. Siebesma, and J. Teixeira, 2004: An eddy-diffusivity/mass-flux parameterization for dry and shallow cumulus convection. *Quart. J. Roy. Meteor. Soc.*, **130**, 3055–3079.
- Stefănescu, S., L. Berre, and M. B. Pereira, 2006: The evolution of dispersion spectra and the evaluation of model differences in an ensemble estimation of error statistics for a limited-area analysis. *Mon. Wea. Rev.*, **134**, 3454–3476.
- Tegen, I., P. Hoorig, M. Chin, I. Fung, D. Jacob, and J. Penner, 1997: Contribution of different aerosol species to the global aerosol extinction optical thickness: Estimates from model results. *J. Geophys. Res.*, **102**, 23 895–23 915.
- Tulet, P., V. Crassier, F. Solmon, D. Guedalia, and R. Rosset, 2003: Description of the mesoscale nonhydrostatic chemistry model and application to a transboundary pollution episode between northern France and southern England. *J. Geophys. Res.*, **108**, 4021, doi:10.1029/2000JD000301.
- , —, F. Cousin, K. Suhre, and R. Rosset, 2005: ORILAM, a three-moment lognormal aerosol scheme for mesoscale atmospheric model: Online coupling into the Meso-NH-C model and validation on the Escompte campaign. *J. Geophys. Res.*, **110**, D18201, doi:10.1029/2004JD005716.
- Vána, F., P. Bénard, J.-F. Geleyn, A. Simon, and Y. Seity, 2008: Semi-Lagrangian advection scheme with controlled damping: An alternative to nonlinear horizontal diffusion in a numerical weather prediction model. *Quart. J. Roy. Meteor. Soc.*, **134**, 523–537.
- Wattrelot, E., O. Caumont, S. Pradier-Vabre, M. Jurasek, and G. Haase, 2008: 1D+3DVar assimilation of radar reflectivities in the pre-operational AROME model at Météo-France. *Fifth Conf. on Radar in Meteorology and Hydrology*, Helsinki, Finland, Finnish Meteorological Institute. [Available online at <http://erad2008.fmi.fi/proceedings/extended/erad2008-0097-extended.pdf>.]
- Wulfmeyer, V., and Coauthors, 2008: The convective and orographically induced precipitation study: A research and development project of the World Weather Research Program for improving quantitative precipitation forecasting in low-mountain regions. *Bull. Amer. Meteor. Soc.*, **89**, 1477–1486.
- Yan, X., V. Ducrocq, G. Jaubert, P. Brousseau, P. Poli, C. Champollion, C. Flamant, and K. Boniface, 2009: Benefit of GPS zenith delay assimilation on high-resolution quantitative precipitation forecast of the COPS CASES IOP9. *Quart. J. Roy. Meteor. Soc.*, **135**, 1788–1800.